Progress In Electromagnetics Research, Vol. 133, 459–475, 2013

SPARSE TIME-FREQUENCY REPRESENTATION BASED FEATURE EXTRACTION METHOD FOR LANDMINE DISCRIMINATION

Y. Wang*, Q. Song, T. Jin, Y. Shi, and X. Huang

School of Electronic Science and Engineering, National University of Defense Technology, Changsha, Hunan 410073, China

Abstract—Low-frequency ultra-wideband synthetic aperture radar is a promising technology for landmine detection. According to the scattering characteristics of body-of-revolution (BOR) along with azimuth angles, a discriminator based on Bayesian decision rule is proposed, which uses sequential features, i.e., double-hump distance. First, the algorithm estimates the target scatterings in all azimuth angles based on regions of interest. Second, sequential aspect features are extracted by sparse time-frequency representation. Third, the distributions of features are obtained by training samples, and then the posterior probability of landmine class is computed as an input to the classifier adopting Mahalanobis distance. The experimental results indicate that the proposed algorithm is effective in BOR target discrimination.

1. INTRODUCTION

Landmines have been widely used in wars for theirs destructive and easily laid, and lots of them are left after the wars. Both of them cause enormous civilian casualties and economic loss [1–3]. So Landmine detection and clearance have become the urgent need to address problem in the view either humanitarian or military applications. But detection and clearance of landmine are known to be an extremely challenging task, which is response to the complexity of environment compounded by soil, weather, terrain, and so on.

Many kinds of sensors are under investigation for landmine detection, e.g., multispectral sensor [4], hyperspectral sensor [5], infrared sensor [6], and ground penetrating radar (GPR) [7]. GPR

Received 21 August 2012, Accepted 19 October 2012, Scheduled 3 November 2012

* Corresponding author: Yuming Wang (yumingwang_1985@yahoo.com.cn).

is a promising technology which can detect both plastic and metal landmines. As a promotion technology of GPR, low-frequency ultra-wideband synthetic aperture radar (LFUWB-SAR) has been an important tool for landmine detection over the last several decades [8–10], which offers the advantage of a significant standoff distance to perform large areas detection quickly from its high resolution image.

Like the classical method of target detection in SAR image [11, 12], landmine detection is often accomplished in two stages. The first stage is prescreening, which extracts some small size images, each of which contains a suspicious target and is denoted as region of interest (ROI), from the large terrain through a simple local gray feature. The second stage is discrimination, which uses the ROI features to distinguish clutters from targets. This method is effective since the prescreening is used to reduce the calculation amount and the discrimination is used to discard false alarms. Because there always exist a large variety of strong scattering clutters in observation scene such as stones, pits, tree trunks, and so on, the major challenge for LFUWB-SAR landmine detection is too many false alarms in final detection results. Therefore, the extraction of features used for discrimination is the key point to reduce false alarm rate.

Features extraction and discrimination have been extensively explored and there are still under investigation in methodological aspect. Gray and geometric features in time domain are always the first consideration to be extracted, like the maximum amplitude of ROI pixel, signal-to-clutter ratio (SCR), double-hump signature, et al.. Spectrum-based features are another consideration due to the wide bandwidth of radar. For example, the features of subbands with good target-to-clutter contrast are input into a classifier designed based on Fischer's linear discriminant in [13]. The time-frequency (TF) analysis [14, 15] can extract the target features of the time domain and the frequency domain simultaneously, which yields a potentially more revealing image of the ROI range components. A lot of discriminators which are suitable for corresponding features have been designed just like the generalized ratio test (GLRT) detector [9] and the hypersphere support vector machine (HS-SVM) [16]. However, these studies do not provide much attention to the azimuth characteristics of target scatterings.

The aim of this paper is to provide a method to extract the features of scattering for landmine discrimination. Due to the wide accumulating angle of azimuth and wide bandwidth of LFUWB-SAR, aspect TF features of scatterings abound with a large amount of target information. At present, the sub-aperture method [17, 18] is the main method to extract the sequential aspect features. At the expense of

image resolution and target SCR, the sub-aperture method leads to the following questions: (1) The more sub-aperture, the worse features accuracy subject to the limitations of SCR and resolution; (2) the fewer sub-aperture, the worse robustness of sequential variation although the features accuracy of single ROI improve.

In fact, the echo can be considered as the accumulation of reflection caused by points which have the same distance from themselves to the radar antenna. So it is difficult to separate the target scatterings from echoes. To address the above issues, we present an algorithm that separates the scatterings using the entire aperture ROI image. The target reflection in the two-dimensional image is relatively stronger than in the one-dimensional echo for coherent accumulation of all azimuth angles. So we can segment the target ROI more easily by prescreening. In terms of imaging mode, we can take advantage of the relation between the image and the echo to reconstruct landmine scatterings. TF analysis is illustrated to be suitable for target subscription, but the conventional TF analysis algorithm is defective just like that Wigner-Ville distribution has cross-components [19]. A sparse TF representation [20, 21] based on the overcomplete dictionary with Gabor atoms is adopted, and the atom parameters are taken as features. Statistic diversity of feature is the significant characteristic between targets and clutters, and it has been widely applied in target discriminating. A discriminator based on Bayesian decision rule is designed using the sequential aspect features (SAF) which consists of sparse TF atoms.

The remainder of this paper is organized as follows. In Section 2, we give a description on the flow of how the scatterings of target are estimated using the entire aperture ROI image. In Section 3, the processing of sequential features extracted by sparse TF is introduced in details. Section 4 discusses the Bayesian decision rule based discriminator via above features. The experimental results are discussed in Section 5. Finally, the conclusion is given in Section 6.

2. SCATTERINGS ESTIMATION

In order to estimate the landmine scatterings, we firstly introduce imaging model in brief. LFUWB-SAR adopts side looking strip imaging mode. The electromagnetic wave transmitting and receiving work in a cycle while the flight states are "go-stop-go". In this mode, as shown in Fig. 1, the direction of radar movement is orthogonal with the antenna beam, where r, x denote the slant range and azimuth position respectively, r-x the imaging plane, and φ the azimuth angle. The constant integration angle back projection (CIABP) algorithm [22]

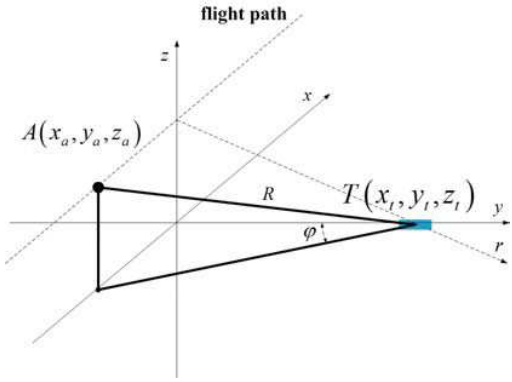

Figure 1. Illustration of three-dimensional imaging geometry model.

is widely used for producing high resolution images in LFUWB-SAR. We take an assumption that $f(r, x)$ is SAR image acquired through CIABP. The target echo is considered as the measurement of scatterings in the frequency-azimuth angle domain, f-φ, with f being frequency. Correspondingly, the imaging algorithm is a function that maps data from f-φ to r-x, and the frequency domain echo $s(f, \varphi)$ can be expressed as $s(t, u)$ in the time domain, where t is fast-time and u is slow-time (or called azimuth aperture position). The CIABP formula is.

$$f(r, x) = \iint t^2 s(t, u) \delta \left(t - \frac{2}{c} R \right) dt du \tag{1}$$

where c is the speed of light, R the distance from antenna to target, and $\delta(\cdot)$ Dirac Delta function.

Based on the CIABP imaging model [23], we have the following relationship as

$$\begin{cases} k = \frac{1}{2}\sqrt{k_x^2 + k_r^2} \\ \varphi = \arctan\left(-\frac{k_x}{k_r}\right) \end{cases} \tag{2}$$

where k_x is the azimuth wave number, k_r the slant wave number, and $k = 2\pi f/c$. The value scope of φ is $[-\frac{\pi}{2}, \frac{\pi}{2})$. Based on (2), we design the flow of scatterings estimation as follows.

- The wave number image is acquired through 2-dimensional fast Fourier transform (2D-FFT) based on target entire aperture ROI, which is expressed as $f(r, x) \rightarrow \bar{S}(k_r, k_x)$.
- We take advantage of (2) to map the $\bar{S}(k_r, k_x)$ into $\hat{s}(f, \theta)$.

- By means of the 1-dimension inverse fast Fourier transform (IFFT) along with the slant range, the $\hat{s}(f,\varphi)$ can be transformed into $\hat{s}(t,\varphi)$.

$\hat{s}(t,\varphi)$ is the estimation of scattering when azimuth angle is φ. The process of obtaining the target ROI is equivalent to be filter in the spatial domain, which can effectively inhibit the response of strong scattering point with the same distance from target to antenna, and then improve the accuracy of the estimation.

3. SPARSE TIME-FREQUENCY REPRESENTATION

There is existing double-dump in landmine reflection in both time domain and frequency domain [24, 25], so its corresponding TF image manifests a "#" structure, which has the sparse characteristic. The sparse TF representation can be rewritten as

$$\hat{s}_{\varphi} = D\boldsymbol{\alpha} \tag{3}$$

where D is overcomplete dictionary made up of TF atoms and $\boldsymbol{\alpha}$ the coefficients vector of the signal projecting in the dictionary. To approximate the signal with fewer non-zero coefficients, (3) can be transformed into an optimization formula:

$$\min_{\alpha} \|\boldsymbol{\alpha}\|_0 \quad s.t. \quad \hat{s}_{\varphi} = D\boldsymbol{\alpha} \tag{4}$$

where $||\cdot||_0$ indicates the norm of ℓ_0.

Gabor atom is a common TF atom [26], which is defined as

$$\begin{cases} g_{\rho}(t) = \frac{1}{\sqrt{a}} g\left(\frac{t-b}{a}\right) e^{i\tau t} \\ G_{\rho}(w) = \sqrt{a} G[a(w-\tau)] e^{-i(w-\tau)b} \end{cases} \tag{5}$$

where both $g(t)$ and $G(w)$ are Gauss function, and $\rho = (a, b, \tau)$ are TF parameters which represent scaling factor, shift factor, and tuning factor, respectively. By the modulation of ρ, we can control the atom resolution in the time and the frequency domains, and also the movement of the atom energy.

For solving the optimal coefficients in (4), the matching pursuit (MP) [27] algorithm is often adopted. The MP algorithm is a heuristic optimization algorithm involving atomic search problem. Taking into account the double-dump characteristics of the landmine reflection in time and frequency domain, the atoms are searched in accordance with this regulation: (1) making traversal in time domain, we are apt to identify the most closely atoms matching the time domain double-dump, which are defined as $\rho_1 = (a_1, b_1, \tau_1)$ and $\rho_2 = (a_2, b_2, \tau_2)$; (2) making traversal in frequency domain, we also want to identify

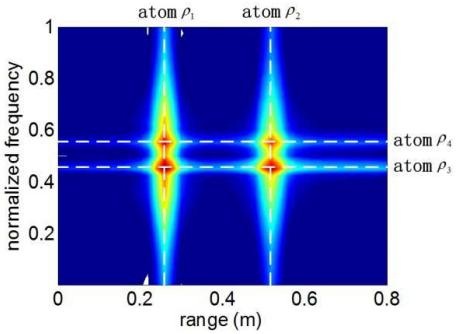

Figure 2. Illustration of using sparse time-frequency representation.

the most closely atoms matching the frequency domain double-dump, which are defined as $\rho_3 = (a_3, b_3, \tau_3)$ and $\rho_4 = (a_4, b_4, \tau_4)$. Fig. 2 shows that the relationship between TF atoms and the double-dump in time or frequency domain. Because a landmine can be considered as a BOR, the double-dump distances in both the time and the frequency domains change regular along with azimuth angles, so we define two variables as $b_{21} = b_2 - b_1$ and $\tau_{43} = \tau_4 - \tau_3$. In terms of [24] and [25], b_{21} and τ_{43} change with the relative position between the antenna and the target. We modify these two features by the factor $\sin\theta$, namely $\rho_b = b_{21}/\sin\theta$ and $\rho_\tau = \tau_{34} \times \sin\theta$, where θ is the indent angle. Let $\boldsymbol{\rho}^\varphi = [\rho_b, \rho_\tau, \rho_1, \rho_2, \rho_3, \rho_4]^H$ be a column vector for the azimuth angle φ, which consists of $I = 14$ features.

For different azimuth angles, we can find different characteristic of landmine scattering. So the SAF are formed by sampling of azimuth angles in order. In this paper, the number of azimuth samples is $N = 11$. Instead of the φ with the number of sampling, the SAF can be defined as $\boldsymbol{\rho}^o = [\boldsymbol{\rho}^1, \boldsymbol{\rho}^2, \ldots, \boldsymbol{\rho}^N]$.

4. DISCRIMINATOR BASED ON BAYESIAN DECISION RULE

In this section, we have the SAF of testing samples except for training samples, and expect to make them classify accuracy. The minimum error of Bayesian decision rule is classical method of discrimination based on class probability density. Furthermore, a target will belong to the class which has the maximum posterior probability. Define the class of landmines is ω_1 and the class of clutters is ω_2.

For each feature in SAF, Kolmogorov-Smirnov (K-S) test algorithm is adopted to obtain its conditional probability distribution [28]. Because landmines have similar characteristics in images and because

clutters have great variety, the distributions of landmines are analyzed. W is the number of landmines samples, and the feature $i(1 \leq i \leq I)$ of sample $w(1 \leq w \leq W)$ in azimuth sample $n(1 \leq n \leq N)$ is $v_n^i(w)$, then the maximum and minimum of samples are obtained via

$$\begin{cases} v_n^i(\max) = \arg\max\limits_{1 \leq w \leq W}(v_n^i(w)) \\ v_n^i(\min) = \arg\min\limits_{1 \leq w \leq W}(v_n^i(w)) \end{cases} \tag{6}$$

We divide $[v_n^i(\min), v_n^i(\max)]$ into equal intervals, where the cell length is $\Delta = \frac{v_n^i(\max) - v_n^i(\min)}{L}$ when the number is L. So the discrete conditional probability $\tilde{P}_{n,i}(l|\omega_1)$ is calculated through

$$\tilde{P}_{n,i}(v_n^i|\omega_1) = \frac{W_\Delta \times L}{(v_n^i(\max) - v_n^i(\min)) \times W} \tag{7}$$

where W_Δ is the number of samples crossed the value l and located in the corresponding cell. Fitting a curve of real data, a continuous probability density function (PDF) $P_{n,i}(v_n^i|\omega_1)$ can be obtained.

We denote a test sample SAF is $v_n^i(t)$, the posterior probability of ω_1 is

$$P_{n,i}(\omega_1|v_n^i(t)) = \frac{P_{n,i}(v_n^i(t)|\omega_1)P(\omega_1)}{P_{n,i}(v_n^i(t))} \tag{8}$$

where $P(\omega_1)$ is the prior probability of ω_1, $P_{n,i}(v_n^i(t))$ the prior probability of $v_n^i(t)$, and the values for both of them are hard to decide. Besides, it is difficult to obtain the posterior probability of ω_2 since the distribution of clutters is unpredictable. In order to solve above problems, we replace $P_{n,i}(\omega_1|v_n^i(t))$ with the value $p_{n,i}(t) = P_{n,i}(v_n^i(t)|\omega_1)$. It can be seen that $p_{n,i}(t)$ is able to express the occurrence probability of ω_1, the higher $p_{n,i}(t)$, the greater the probability of occurrence, on the contrary, the smaller probability of occurrence. For simplicity, the following derivation still uses the concept of probability.

Each row in SAF contains an azimuth sequence of feature (ASF) which appears in order. It is a matter of observation that test sample has more possibilities of being classified in ω_1 when every feature in ASF has higher $p_{n,i}(t)$, so the multiple multiplication method is used to combine all ASFs. The function can be expressed as

$$P(\omega_1|v^i(t)) = \prod_{n=1}^{N} p_{n,i}(t) = \prod_{n=1}^{N} P(v_n^i(t)|\omega_1) \tag{9}$$

where $P(\omega_1|v^i(t))$ is consideration as azimuth posterior probability which depicts the possibility of test sample fell in ω_1.

On the basis of (9), we calculate the azimuth posterior probability of each SAF in $\boldsymbol{\rho}^o$. All $P(\omega_1|v^i(t))$ $(1 \leq i \leq I)$ will constitute a new feature vector $\mathbf{v}$. According to the extraction method, all features have similar accuracy for target description. So we make a classification with the combination of features using the Mahalanobis distance [29]. The new feature vector of training samples is written as $\mathbf{V} = \{\mathbf{v}_1, \mathbf{v}_2, \ldots, \mathbf{v}_W\}$. Calculate the samples covariance matrix

$$\zeta = \frac{1}{M-1} \sum_{m=1}^{M} (\mathbf{v}_m - \bar{\mathbf{v}}) (\mathbf{v}_m - \bar{\mathbf{v}})^T \tag{10}$$

where $\bar{\mathbf{v}}$ is the mean of samples $\mathbf{v}_m (1 \leq m \leq W)$, $\bar{\mathbf{v}} = \frac{1}{W} \sum_{m=1}^{W} \mathbf{v}_m$. The Mahalanobis distance between a sample and the samples set is given by

$$d(\mathbf{v}_m, \bar{\mathbf{v}}) = \sqrt{(\mathbf{v}_m - \bar{\mathbf{v}})^T \zeta^{-1} (\mathbf{v}_m - \bar{\mathbf{v}})} \tag{11}$$

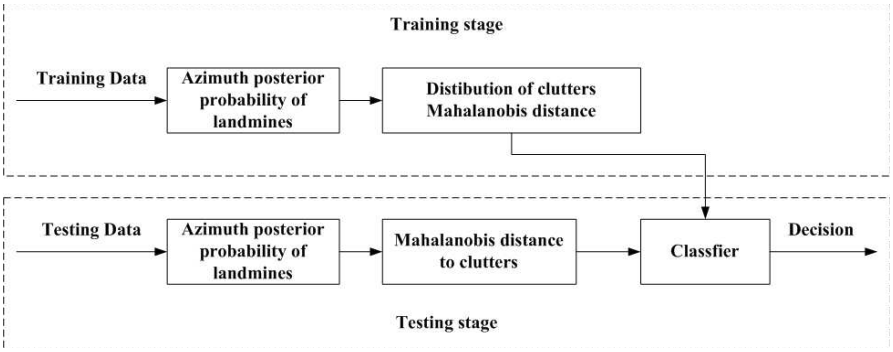

Figure 3. The procedure of discriminator based on Bayesian decision rule.

Figure 4. The AMUSAR system.

In comparison with target, clutter scatterings have dramatic changes all over the azimuth angles, and the corresponding values of $P(\omega_1|v^i(t))$ are smaller. So the discarding of clutters can be considered as one class classification problem. We make assumption that there exists a hypersphere around clutters samples set, and the radius of hypersphere is designed by the distribution of Mahalanobis distances from all clutters to the clutters' centre. Define d_T to be the radius of hypersphere. When $\mathbf{v}_t$ is a test sample, it can be classified via

$$\begin{cases} d(\mathbf{v}_t, \bar{\mathbf{v}}) > d_T, & \mathbf{v}_t \in \omega_1 \\ d(\mathbf{v}_t, \bar{\mathbf{v}}) \leq d_T, & \mathbf{v}_t \in \omega_2 \end{cases} \tag{12}$$

Figure 3 depict the processing of the discriminator.

5. EXPERIMENTAL RESULTS

To demonstrate the effectiveness of the proposed discriminator, the experimental results based on the measured data of Airship-Mounted UWB SAR (AMUSAR) [30] are presented. The AMUSAR system shown in Fig. 4 was developed in 2010 in China. AMUSAR equipped a miniature stepped-frequency SAR with bandwidth of 2 GHz. The SAR image resolution is 0.02 m. We collect total 325 landmines chips

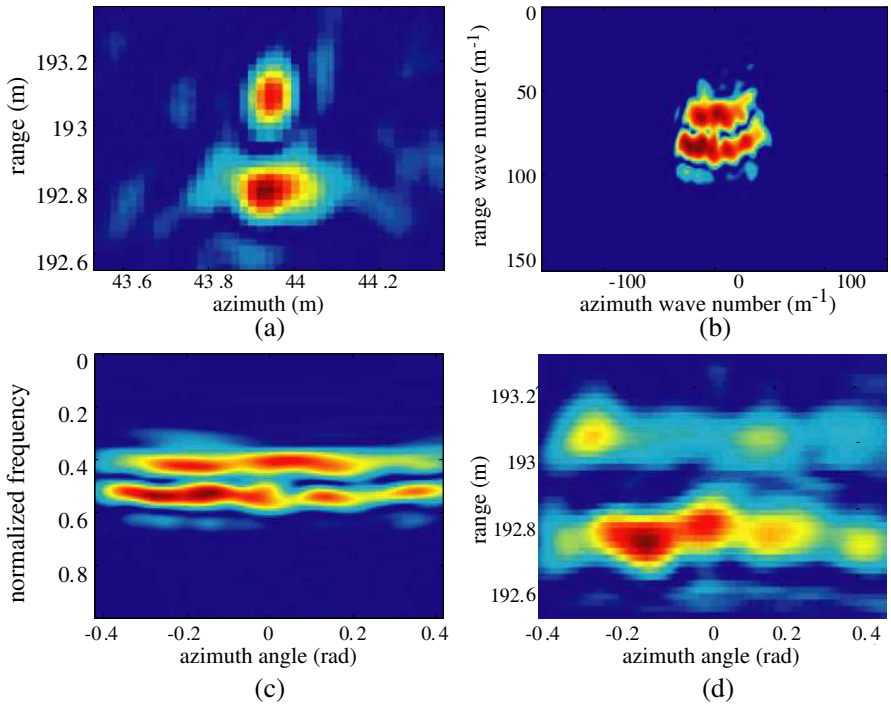

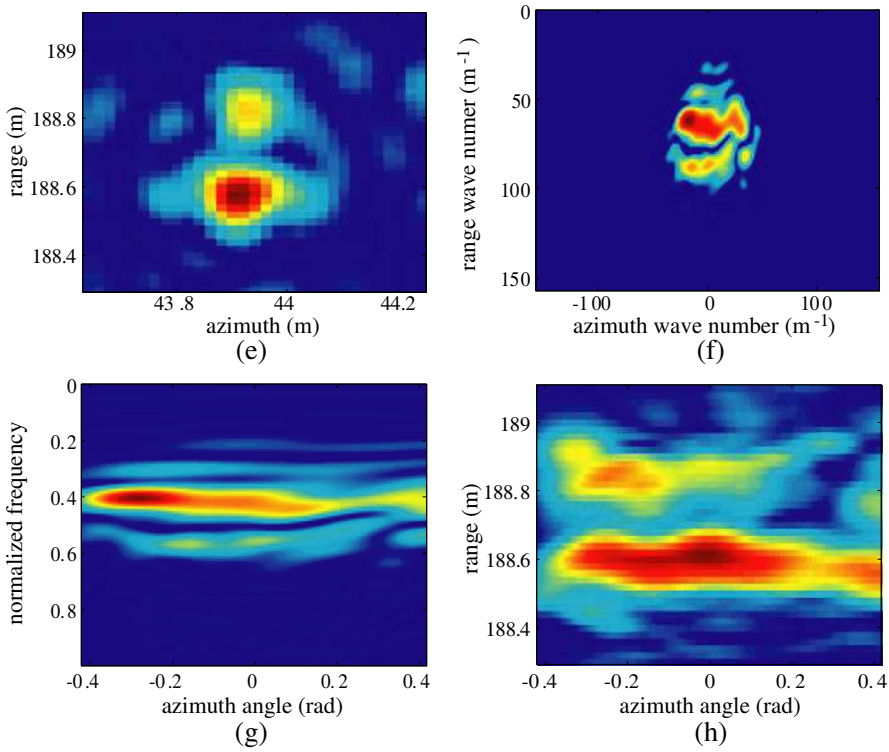

Figure 5. The intermediate processing images of scatterings estimation for landmine and clutter. (a) Original landmine ROI image (size: 41×41 pixels). (b) The k_x-k_r domain image of (a). (c) The f-φ domain image of (a). (d) The t-φ domain image of (a). (e) Original clutter ROI image (size: 41×41 pixels). (f) The k_x-k_r domain image of (e). (g) The f-φ domain image of (e). (h) The t-φ domain image of (e).

and 1252 clutters chips. The landmines samples are collected manually and the clutters samples collected based on the outputs of consistent constant false alarm rate (CFAR) detector [31].

Figure 5 shows the intermediate processing images of scatterings estimation for landmine and clutter respectively. The landmine ROI and clutter ROI have similar structures (Fig. 5(a) and Fig. 5(e)). But the landmine is a BOR, and the scatterings change regularly along with incident angles induced by azimuth angles. Generally, clutters, especially man-made objects, have dihedral angles structure, which is quite different from landmines. Correspondingly, the variant characteristics of scatterings for landmine and clutter are different.

This concept is illustrated in Fig. 5, and Fig. 6 shows further evidence of it. Fig. 6 gives three sparse TF representations for Fig. 5(d) and Fig. 5(h) respectively when the azimuth angles are -0.2, 0, and 0.2. As shown in Fig. 6, the sparse TF images of landmine have similarities in different azimuth angles, but there exits huge change for clutter.

In this paper, the procedure of features processing consists of three steps. First, features are extracted by sparse TF representation of scatterings. Second, SAF are acquired by the combination of features which are sampled in 11 azimuth angles. Third, the new features vector

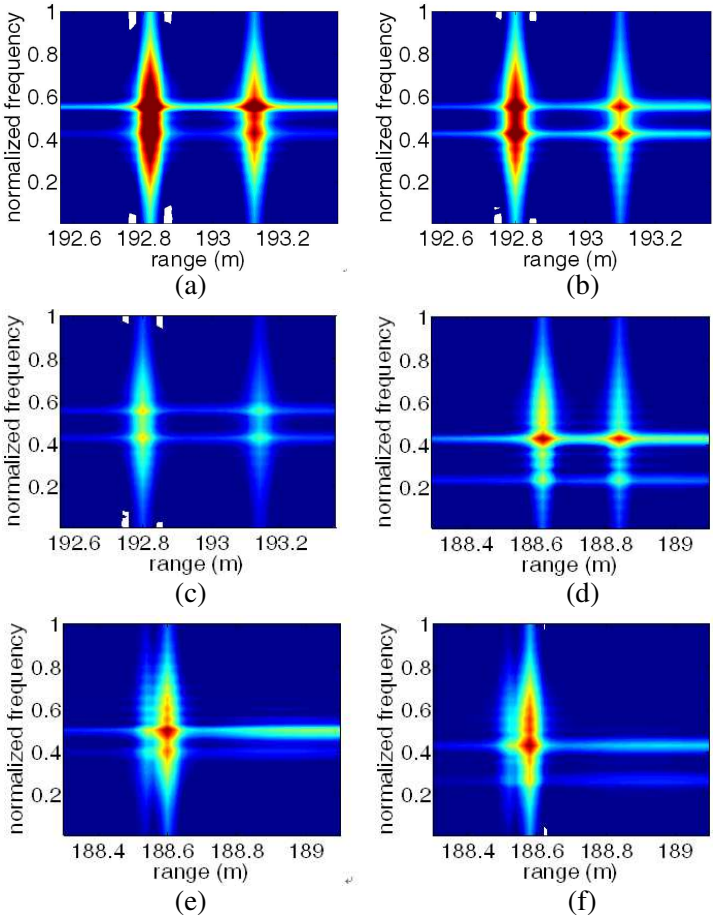

Figure 6. The corresponding sparse TF representations of ROIs in. Fig. 5. (a) Landmine ROI, $\varphi = -0.2$. (b) Landmine ROI, $\varphi = 0$. (c) Landmine ROI, $\varphi = 0.2$. (d) Clutter ROI, $\varphi = -0.2$. (e) Clutter ROI, $\varphi = 0$. (f) Clutter ROI, $\varphi = 0.2$.

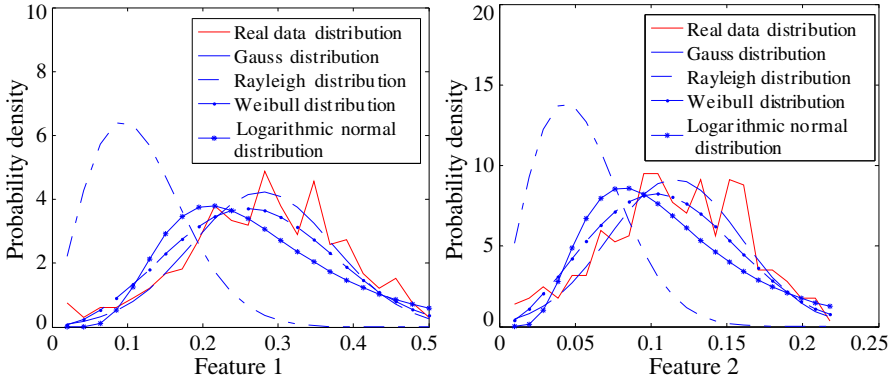

Figure 7. The real data distributions of feature 1 and feature 2 in $\boldsymbol{\rho}^{\varphi}$ ($\varphi = 0$) and classical.

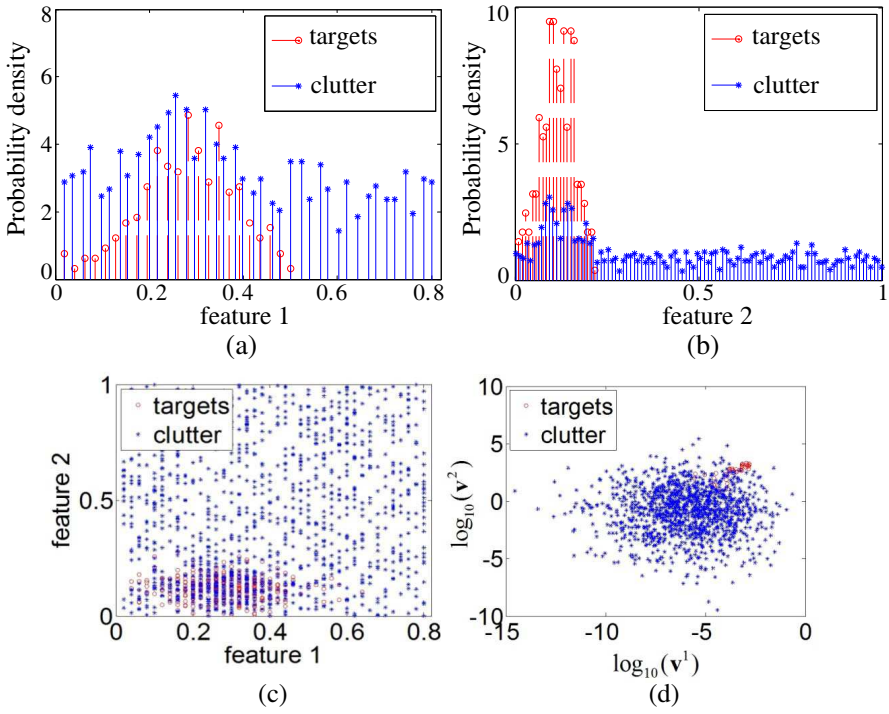

Figure 8. The procedure of features evolution in this paper. (a) The first feature distribution in $\boldsymbol{\rho}^{\varphi}(\varphi = 0)$. (b) The second feature distribution in $\boldsymbol{\rho}^{\varphi}$ ($\varphi = 0$). (c) Combination distribution of the first feature and the second feature in $\boldsymbol{\rho}^{\varphi}$ ($\varphi = 0$). (d) Combination logarithm distribution of the first feature and the second feature in $\mathbf{V}$.

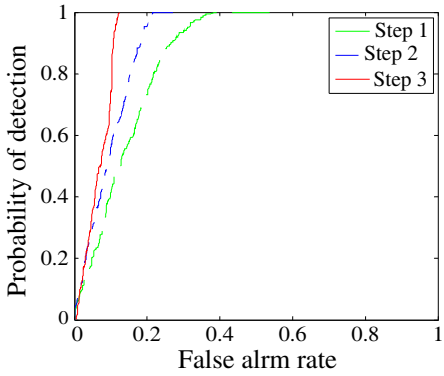

Figure 9. ROC curves for different scenarios.

Table 1. The MSE between real data distribution and classical probability density functions.

Feature type	Gauss	Rayleigh	Weibull	Logarithmic normal
Feature 1	0.52	3.21	0.64	0.96
Feature 2	1.34	6.51	1.62	2.34

is formed in the discriminator based on Bayesian decision rule.

In order to analyze the distribution of features in SAF, we adopt the mean square error (MSE) to refine the approximation between real data distribution and classical PDFs. Define the real data distribution c_1, and the classical probability density function is c_2. Then the MSE between them can be written as $c_{mse} = \|c_1 - c_2\|_2$, where $||\cdot||_2$ indicates the norm of ℓ_2. As seen from Fig. 7, the classical PDFs contain Gauss, Rayleigh, Weibull and Logarithmic normal [32, 33]. Table 1 shows that Gauss function has the minimum MSE with the distributions of feature 1 and feature 2.

From Figs. 8(a)–(c), we can see that landmines can hardly been separated from clutters especially when many clutters have similar features' values to landmines. But in Fig. 8(d), most clutters are far away from the landmines through the three steps mapping of features, where $\mathbf{v}^1$, $\mathbf{v}^2$ are the first and second features in $\mathbf{V}$, respectively. With the comparison of performances of features extracted in different steps, Fig. 9 gives their receiver operator characteristic (ROC) curves. As expected, the discriminator, proposed in this paper, produces the best of the results.

6. CONCLUSION

In this paper, accurate extraction of the scatterings is the key of the landmine discrimination. As a BOR, the landmine scatterings change regularly, and there are differences with the clutter azimuth scatterings. First, this paper analyzes the relationship between entire aperture ROI image and the scatterings of target, and then extracts SAF using sparse TF representation. Second, a discriminator based on the Bayesian decision rule has been designed. The posterior probabilities of landmines class are calculated to discriminate suspicious targets with SAF, and the Mahalanobis distance adopted for the final classification easily achieves a good performance. The real data results show that the method through three steps of features extraction or transformation can effectively improve the performance of discrimination.

ACKNOWLEDGMENT

This work was supported by the National Natural Science Foundation of China under Grants 60972121 and 61271441; the Foundation for the Author of National Excellent Doctoral Dissertation of China under Grant 201046; the Program for New Century Excellent Talents in University under Grant NCET-10-0895; the research project of NUDT CJ12-04-02.

REFERENCES

1. Habib, M. K., "Humanitarian demining: Reality and the challenge of technology-the state of the arts," *International Journal of Advanced Robotic Systems*, Vol. 4, No. 2, 151–172, 2007.
2. Tiwari, K. C., D. Singh, and M. K. Arora, "Development of a model for detection and estimation of depth of shallow buried non-metallic landmine at microwave X-band frequency," *Progress In Electromagnetics Research*, Vol. 79, 225–250, 2008.
3. International Campaign to Ban Landmines Monitor Report: Toward a Mine-Free World, 2006.
4. Lange, D. J. and E. Breejen, "Airborne multi-spectral minefield survey," *Advanced Sensory Payloads for UAV*, 18-1–18-8, 2005.
5. McFeea, J. E., et al., "Landmine detection using passive hyperspectral imaging," *Proc. of SPIE*, Vol. 6554, 655404-01–655404-13, 2007.
6. Cremer, F., et al., "Stand-off thermal IR minefield survey: System

concept and experimental results," *Proc. of SPIE*, Vol. 5794, 209–220, 2005.

7. Moustafa, K. and K. F. A. Hussein, "Performance evaluation of separated aperture sensor GPR system for land mine detection," *Progress In Electromagnetics Research*, Vol. 72, 21–37, 2007.
8. Moussally, G., R. Fries, and R. Bortins, "Ground-penetrating synthetic-aperture radar for wide-area airborne minefield detection," *Proc. of SPIE*, Vol. 5415, 1042–1052, 2004.
9. Kositsky, J., R. Cosgrove, and C. Amazeen, "Results from a forward-looking GPR mine detection system," *Proc. of SPIE*, Vol. 4394, 700–711, 2001.
10. Bradley, M., et al., "Mine detection with a forward-looking ground-penetrating synthetic aperture radar," *Proc. of SPIE*, 334–347, 2003.
11. Chang, Y.-L., C.-Y. Chiang, and K.-S. Chen, "SAR image simulation with application to target recognition," *Progress In Electromagnetics Research*, Vol. 119, 35–57, 2011.
12. Gao, G., et al., "Fast detecting and locating groups of targets in high-resolution SAR images," *Pattern Recognition*, Vol. 40, 1378–1384, 2007.
13. Wang, T. P., et al., "Frequency subband processing and feature analysis of forward-looking ground-penetrating radar signals for land-mine detection," *IEEE Transactions on Geoscience and Remote Sensing*, Vol. 45, No. 3, 718–729, 2007.
14. Sun, Y. J. and J. Li, "Plastic landmine detection using time-frequency analysis for forward-looking ground penetrating radar," *Proceedings of SPIE*, Vol. 5089, 851–862, 2005.
15. Han, S.-K., H.-T. Kim, S.-H. Park, and K.-T. Kim, "Efficient radar target recognition using a combination of range profile and time-frequency analysis," *Progress In Electromagnetics Research*, Vol. 108, 131–140, 2010.
16. Jin, T., et al., "The evidence framework applied to fuzzy hypersphere SVM for UWB SAR landmine detection," *Proceedings of ICSP*, Vol. 3, 16–20, 2006.
17. Liao, K.-F., X.-L. Zhang, and J. Shi, "Fast 3-D microwave imaging method based on subaperture approximation," *Progress In Electromagnetics Research*, Vol. 126, 333–353, 2012.
18. Ji, S. H., R. Parr, and L. Carin, "Nonmyopic multiaspect sensing with partially observable Markov decision processes," *IEEE Transactions on Signal Processing*, Vol. 55, No. 6, 2720–2730, 2007.

19. Chu, X., "Evolution of beam quality and shape of Hermite-Gaussian beam in non-Kolmogorov turbulence," *Progress In Electromagnetics Research*, Vol. 120, 339–353, 2011.
20. Zhu, M., et al., "A time-frequency atom approach to radar emitter signal feature extraction," *Communications, Circuits and Systems Proceedings*, Vol. 1, 615–619, 2006.
21. Rodriguez, I. V., D. Bonar, and M. S. Sacchi, "Microseismic record de-noising using a sparse time-frequency transform," *SEG Annual Meeting*, 1–6, 2011.
22. Rau, R. and J. H. McClellan, "Analytic models and postprocessing techniques for UWB SAR," *IEEE Transactions on Aerospace and Electronic Systems*, Vol. 36, No. 4, 1058–1074, 2000.
23. Jin, T., Z. M. Zhou, and W. G. Chang, "Man-made targets pose estimation using time-frequency distribution in UWB SAR," *Geoscience and Remote Sensing Symposium, IGARSS*, Vol. 7, 4633–4635, 2005.
24. Vitebskiy, S., L. Carin, and M. A. Ressler, "Ultra-wideband, short-pulse ground-penetrating radar: Simulation and measurement," *IEEE Transaction on Geoscience and Remote Sensing*, Vol. 35, No. 3, 762–77, 1997.
25. Jin, T. and Z. M. Zhou, "Feature extraction and discriminator design for landmine detection on double-hump signature in ultrawideband SAR," *IEEE Transactions on Geoscience and Remote Sensing*, Vol. 46, No. 11, 3783–3791, 2008.
26. Ma, S. W., et al., "Parametric adaptive time-frequency representation based on time-sheared Gabor atoms," *Journal of Systems Engineering and Electronics*, Vol. 18, No. 1, 1–7, 2007.
27. Li, J., S. Zhang, and J. Chang, "Applications of compressed sensing for multiple transmitters multiple azimuth beams SAR imaging," *Progress In Electromagnetics Research*, Vol. 127, 259–275, 2012.
28. Conte, E., A. Demaio, and C. Galdi, "Statistical analysis of real clutter at different range resolutions," *IEEE Transaction on Aerospace and Electronic Systems*, Vol. 40, No. 3, 903–918, 2004.
29. Xiang, S. M., F. P. Nie, and C. S. Zhang, "Learning a mahalanobis distance metric for data clustering and classification," *Pattern Recognition*, Vol. 41, No. 12, 3600–3612, 2008.
30. Song, Q., et al., "Results from an airship-mounted ultra-wideband synthetic aperture radar for penetrating surveillance," *Asia-Pacific Conference on Synthetic Aperture Radar*, 194–197, Seoul, Korea, 2011.

31. Habib, M. A., M. Barkat, B. Aïssa, and T. A. Denidni, "Ca-CFAR detection performance of radar targets embedded in 'non centered Chi-2 gamma' clutter," *Progress In Electromagnetics Research*, Vol. 88, 135–148, 2008.
32. Pinel, N., C. Bourlier, and J. Saillard, "Forward radar propagation over oil slicks on sea surfaces using the ament model with shadowing effect," *Progress In Electromagnetics Research*, Vol. 76, 95–126, 2007.
33. Owolawi, P. A., "Rainfall rate probability density evaluation and mapping for the estimation of rain attenuation in South Africa and surrounding islands," *Progress In Electromagnetics Research*, Vol. 112, 155–181, 2011.